Highly sensitive humidity measurement with temperature compensation based on a special dual-modal interferometric sensor and varied period Vernier effect

Yunqing Guan, Matthias Fabian, Xiaopeng Dong, Hongwei Gao, Yingbin Feng, Tong Sun, and Kenneth T. V. Grattan

***Abstract*—This paper proposes a novel highly sensitive humidity sensor with temperature compensation, mainly consisting of a special modal interferometer bonded with thick polyimide (PI) solid films. The modal interferometer is constructed by splicing a special dual-mode fiber (DMF) with two sections of regular single mode fiber (SMF), forming an SDS (SMF-DMF-SMF) structure. Due to the particular design of the refractive index of the DMF, only LP_{01} and LP_{02} modes are transmitted, which causes a unique wavelength (UWL) to appear in the spectrum. The UWL breaks the periodicity of the conventional interferometric spectrum. More importantly, both sides of UWL respond differently to various measurands, which enables the interferometer to measure dual parameters simultaneously. To achieve a higher humidity sensitivity, the thick PI solid films are used for the first time to manufacture the interferometric humidity sensors. Their thickness is at least one order of magnitude greater than that of the PI coating used in the traditional humidity sensors, which enhances the sensor's response to humidity variation significantly. The performance of the proposed sensor is further improved with the aid of the varied period Vernier effect by paralleling a bare dual modal interferometer based on the SDS structure as a reference. Similar to the sensing modal interferometric spectrum, the output spectrum of the varied period Vernier effect scheme owns the UWL as well, which makes it easy to distinguish the wavelength shifts of the specific peaks to the measurands. The validity of the proposed scheme is verified by an experimental case, where the humidity sensitivity and the temperature sensitivity are achieved as 1044.26 pm/%RH and 1467.99 pm/°C, respectively.**

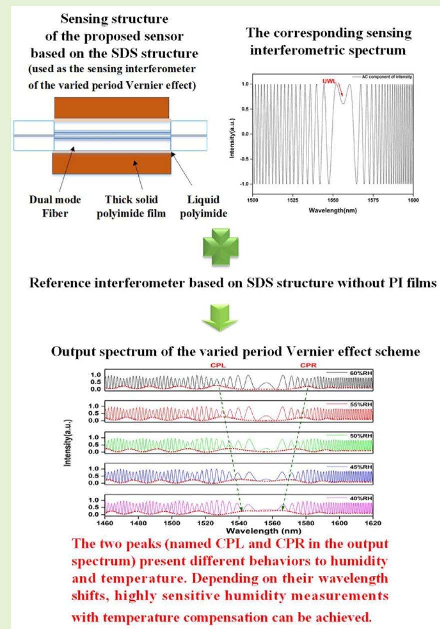

***Index Terms*—special dual-mode fiber, unique wavelength, thick polyimide solid films, varied period Vernier effect.**

I. Introduction

Humidity is a critical parameter that signifies the moisture content in the air. Over time, numerous approaches have been put forth to accomplish the highly sensitive humidity measurements in diverse applications. These applications include but are not limited to respiration detection [1], nondestructive testing [2], high energy physics [3] etc. Among them, optical fiber sensors are immune to electromagnetic interference and do not require an electrical power supply, which makes them particularly suitable for practical measurements [4].

The well-known Fiber Bragg grating (FBG) coated with moisture-sensitive materials, such as PI, represents a typical type of humidity sensor with a compact size that can be easily fitted in small areas [5]. The stretching or contracting of the PI coating affected by humidity variation induces strain on the FBG and shifts its center wavelength. However, the humidity sensitivity (usually a few pm per %RH) is limited by the thickness of the coating. Besides, this type of sensor based on PI coating is often manufactured through the dip coating method [6], which presents the following drawbacks. First, to ensure each PI layer can be coated uniformly on the fiber, the coating machines are usually set at a very slow speed (for

This work was supported by the Introduction Programme for High-level Talents of Shenyang LiGong University, Liaoning Province Joint Open Fund for Key Scientific and Technological Innovation Bases under Grant 2021-KF-12-05, Basic scientific research project of Liaoning Provincial Department of Education under Grant LJKMZ20220614.

Yunqing Guan and Yingbin Feng are with the School of Automation and Electrical Engineering, Shenyang Ligong University, Shenyang 110159, China. (email: yunqingguan@sylu.edu.cn; 781787793@qq.com). Hongwei Gao is with the Institute of International Engineering, Shenyang LiGong University, Shenyang 110159, China. (email: 30963915@qq.com). Matthias Fabian and Tong Sun are with the School of Mathematics, Computer Science and Engineering, City, University of London, London EC1V 0HB, U.K.(e-mail: matthias.fabian.1@city.ac.uk; t.sun@city.ac.uk). Xiaopeng Dong is with the School of Electronic Science and Engineering, Institute of Lightwave Technology, Xiamen University, Xiamen 361005, and also with Key Laboratory for Optical Communication Device Test of Xiamen.(email: xpd@xmu.edu.cn). Kenneth T. V. Grattan is with the City Graduate School, City, University of London, London EC1V 0HB, U.K., and also with the School of Mathematics, Computer Science and Engineering, City, University of London, London EC1V 0HB, U.K.(e-mail: k.t.v.grattan@city.ac.uk). Corresponding author: Hongwei Gao, Yingbin Feng.

example, 13 mm/minute in [7]), then to make each PI layer and fiber bond tightly, the sensing area needs to be placed in the oven for several minutes at 150 °C, prior to the next dip coat, and followed by final curing at 180 °C for 60 minutes [7]. Thus, to produce a humidity sensor with multiple PI layers, the fabrication process is rather complicated and time-consuming. Second, the dip coating method often necessitates immersing one end of the FBG into the humidity-sensitive material. This complicates the process of connecting the FBG humidity sensors in series, compromising the inherent advantage of the ease of multiplexing for FBG sensors and impeding their practical application in monitoring humidity at multiple points. Consequently, the need for more efficient fabrication methods for humidity sensors is still highly demanding.

In comparison to the FBG humidity sensors, interferometric optical fiber humidity sensors exhibit superior sensitivity [8]. The prevailing demodulation method for these sensors involves measuring the response of the peaks or valleys at specific wavelengths to humidity variations [9]. However, practical applications necessitate consideration of temperature disturbance, as it has a certain correlation with humidity. Conventional interferometric spectra generally exhibit periodic fringes, which present similar responses to both humidity and temperature variations. Additionally, a majority of moisture-sensitive materials, including PI, demonstrate analogous responses to changes in temperature as they do to variations in humidity. Thus, it is hard to distinguish humidity variation and temperature variation solely from the wavelength shifts of the sensing spectra, rendering traditional interferometric sensors incapable of measuring humidity and temperature simultaneously. Connecting a bare FBG in series with a humidity sensor can solve the problem to some extent [10]. Nevertheless, the error cannot be ignored, as the humidity sensor and the FBG for temperature compensation cannot share the same location. To eliminate the cross-sensitivity of the sensor, the intensity demodulation method is often combined with the wavelength tracking method, which leads to additional consideration of any factor that causes the fluctuation in optical power [11]. Therefore, realizing highly sensitive humidity measurement with temperature compensation remains a challenge.

To overcome these problems, a DMF-based interferometer bonded with thick PI films is proposed in this paper. Based on our previous studies, only LP_{01} and LP_{02} modes propagate in the DMF and exhibit stable interference [12]. The propagate constant difference of the two modes, denoted by Δβ, varies non-monotonically with the wavelength, and the wavelength corresponding to the maximum value of Δβ is called UWL, which breaks the periodicity of the spectrum. The spectra on both sides of the UWL show different behaviors towards humidity and temperature, which can be amplified with the combination of the Vernier effect. In addition, considering the sensitivity of the humidity sensor coated with PI highly depends on the coating thickness, the novel material, i.e. thick PI film, is utilized with sub-millimeter thickness, which is at least an order than that of the traditional PI coating. The response to the humidity of the sensor is greatly enhanced and the corresponding fabrication method is much more efficient.

II. Sensing Structure And Measurement Principle

The DMF (Provided by Yangtze Optical Fiber and Cable Joint Stock Limited Company) is specially designed with a highly GeO_2-doped core zone and cladding zones with different refractive indices, enabling it to support the transmission of only LP_{01} and LP_{02} modes within its core. The cross-section image of the DMF obtained by the scanning electron microscope (SEM) is shown in Fig. 1.

To express the refractive index in a more general way, the normalized refractive index difference $\Delta n_{core/claddingi}$ can be defined as Eq. (1):

$$\Delta n_{core/claddingi} = (n_{core/claddingi} - n_0)/n_0 \quad (1)$$

Where $n_{core/claddingi}$ represents the refractive indices of the core or the i th inner cladding and n_0 represents the refractive index of the outermost pure silica layer, respectively. The normalized refractive index difference distribution of the cross-section is shown in Table I:

TABLE I
THE NORMALIZED REFRACTIVE INDEX DIFFERENCE DISTRIBUTION OF THE CROSS-SECTION OF THE DMF.

Position of the cross-section	Radius range (μm)	Normalized refractive index difference
Core	0 ~ 4	Δn_{core}=1.99%
First inner cladding	4 ~ 7.15	$\Delta n_{cladding1}$=–0.40%
Second inner cladding	7.15 ~ 9	$\Delta n_{cladding2}$=0.48%
Third inner cladding	9 ~ 15	$\Delta n_{cladding3}$=0.14%
Outer cladding	15 ~ 62.5	-

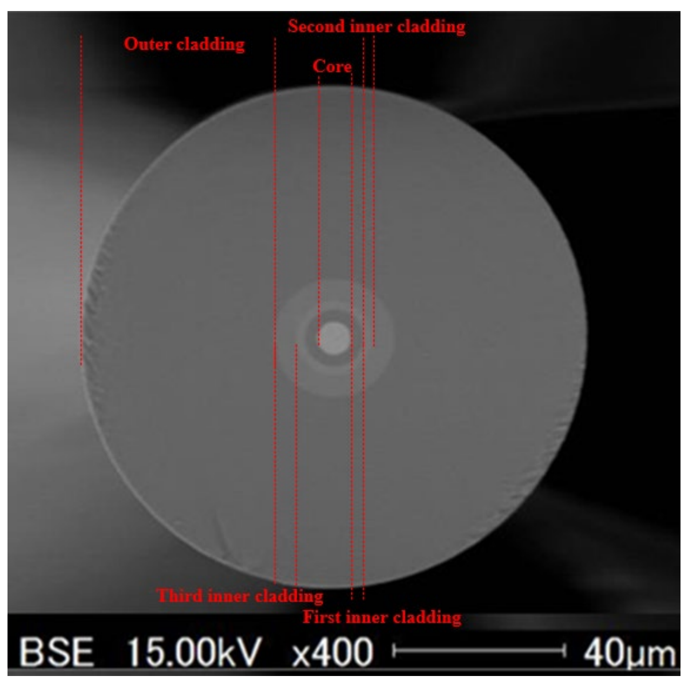

Fig.1. The SEM image of the cross-section of DMF.

Both ends of the DMF can be fused with SMF to form the SDS structure interferometer. Due to the special design of the

DMF, only LP_{01} mode and LP_{02} mode are excited by the fundamental mode of the input SMF, propagating exclusively within the DMF core. The interference signal is then transmitted by the output SMF. e_1 and e_2 are used to represent the excitation efficiency of the LP_{01} mode and LP_{02} mode, respectively. Then, the intensity of the transmission spectrum, I_T, and its AC component, I_{T_AC}, can be expressed as [13]:

$$I_T = {e_1}^2 + {e_2}^2 + 2e_1e_2cos\varphi_\lambda, I_{T\_AC} = cos\varphi_\lambda \tag{2}$$

Where φ_λ represents the phase difference between the two modes, it can be further given as:

$$\varphi_\lambda = \Delta\beta L = \frac{2\pi\Delta n_{eff}L}{\lambda} \tag{3}$$

Where L is the length of the DMF and Δn_{eff} is the efficient refractive index difference. The simulated curve of Δn_{eff} vs. λ can be obtained with the help of a finite element analysis model built by the software COMSOL, depicted in Fig. 2(a). Subsequently, $\Delta\beta$ and I_{T_AC} can be calculated using Eq. (3) and Eq. (2), respectively, as illustrated in Fig. 2(b).

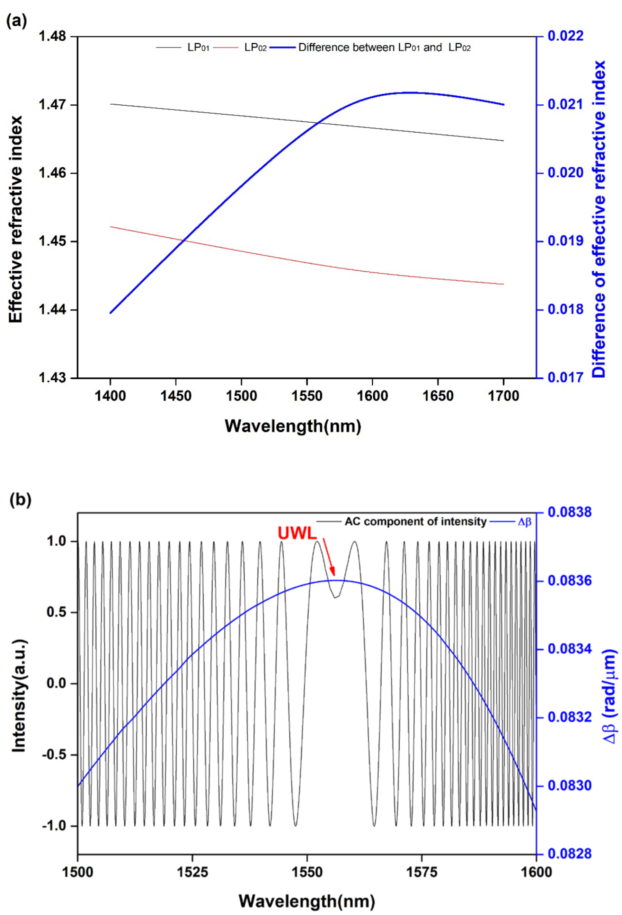

Fig.2. (a) The simulated curves of efficient refractive indices of LP_{01} and LP_{02}, and the difference between them. (b) The simulated curve of Δβ and the simulated spectrum of the dual modal interferometer (L = 20 cm).

It is evident from Fig. 2(a) and Fig. 2(b) that the variations in Δn_{eff} and $\Delta\beta$ exhibit non-monotonic behaviors with respect to λ. These behaviors stand in stark contrast to that of the modal interferometer based on the conventional dual-mode fiber [14]. Consequently, the wavelength corresponding to the relative maximum value of $\Delta\beta$ ($\lambda_{\Delta\beta\_max}$) possesses distinctive characteristics and is denoted as UWL in Fig. 2(b). This wavelength can be further expressed as $UWL = \lambda_{\Delta\beta\_max}$. The appearance of the UWL breaks the periodicity of the interferometric spectrum. Additionally, when the measurand varies, the wavelengths on both sides of UWL will shift in opposite directions, due to the different monotonicity of $\Delta\beta$ on each side of UWL. If the wavelengths respond differently to another measurand compared with the former one, it enables the simultaneous measurement of dual parameters.

As the bare fiber sensors are insensitive to the humidity variation, the moisture-sensitive material, such as PI, is selected to be coated on the sensing area of the fiber on most occasions. The strain ε_{RH} will be applied to the fiber when the PI coating stretches or contracts caused by the humidity variation, which can be written as [15]:

$$\varepsilon_{RH} = \left[\frac{A_pE_p}{A_pE_p+A_fE_f}\right](\alpha_{pRH} - \alpha_{fRH})\Delta RH \tag{4}$$

Where A_p and A_f are the cross-sectional areas of the PI coating and fiber, while the subscripts p and f represent the PI and the fiber, respectively. Further, E_p and E_f are Young's modulus of the two materials, respectively, α_{pRH} and α_{fRH} are the moisture expansion coefficients of the two materials, and ΔRH is the relative humidity variation. Based on Eq. (4), there exists a positive correlation between ε_{RH} and A_p, signifying that the increase in A_p enhances ε_{RH}. Nevertheless, the thickness of the traditional PI coating only can reach several micros, which generally limits the humidity sensitivity to several pm/%RH [6], [7].

To improve humidity sensitivity, a novel material called PI film is used to manufacture the proposed humidity sensor. The PI solid film can be produced by the polyamide acid (PAA) solution, followed by a series of steps such as drying and quenching, its sub-millimeter thickness is at least one order of magnitude greater than that of the traditional PI coating used in other humidity sensors [6]. This substantial increase in thickness greatly enhances the strain applied to the fiber when humidity varies, leading to an improvement in humidity sensitivity. In terms of the manufacturing process for the proposed sensor, the sensing area is sandwiched between two pieces of PI film and the liquid PI of the same material is used as the adhesive to ensure a uniform strain transfer. In contrast to the traditional PI coating method outlined in the INTRODUCTION part, this streamlined manufacturing approach improves efficiency significantly. The corresponding structure of the proposed sensor is shown in Fig. 3.

When the sensor is subjected to a change of the measurand χ, the variation of φ_λ, i.e. $\Delta\varphi_\lambda$, can be expressed as [16]:

$$\Delta\varphi_{\lambda} = \frac{\partial\varphi_{\lambda}}{\partial\lambda}\Delta\lambda + \frac{\partial\varphi_{\lambda}}{\partial\chi}\Delta\chi \quad (5)$$

Where $\Delta\lambda$ and $\Delta\chi$ are the variations of λ and χ, respectively. As for tracking the wavelength of a specific peak or dip in the spectrum, such as the peak or dip nearest the UWL, its phase remains a constant, i.e. $\Delta\varphi_{\lambda} = 0$. To be specific, when temperature T varies, the temperature sensitivity S_T can be given as:

$$S_T = \frac{\Delta\lambda}{\Delta T} = -\frac{1}{L}\left(\frac{\partial\Delta\beta}{\partial T}L + \frac{\partial L}{\partial T}\Delta\beta\right)\left(\frac{\partial\Delta\beta}{\partial\lambda}\right)^{-1} \quad (6)$$

Where ΔT is the variation of temperature. Moreover, $\frac{\partial L}{\partial T}$ can be expressed by the strain ε_T caused by the temperature variation, which can be written as [17]:

$$\varepsilon_T = \left[\frac{A_p E_p}{A_p E_p + A_f E_f}\right](\gamma_{pT} - \gamma_{fT})\Delta T \quad (7)$$

Where γ_{pT} and γ_{fT} are the thermal expansion coefficients of the PI material and fiber, respectively. Thus, S_T can be deduced as:

$$S_T = -\left\{\frac{\partial\Delta\beta}{\partial T} + \Delta\beta\left[\left(\gamma_{pT} - \gamma_{fT}\right)\frac{A_p E_p}{A_p E_p + A_f E_f}\right]\right\}\left(\frac{\partial\Delta\beta}{\partial\lambda}\right)^{-1} \quad (8)$$

Similarly, the humidity sensitivity S_{RH} can be deduced as Eq. (9) according to Eq. (4) when humidity varies:

$$S_{RH} = -\left[\frac{A_p E_p}{A_p E_p + A_f E_f}\right]\alpha_{pRH}\left\{\Delta\beta + \frac{k_0^2}{2\beta_{01}\beta_{02}}\left\{\eta\left[\begin{matrix} n_0^4(\beta_{01} - \beta_{02}) \\ +(n_{core}{}^4 - n_0^4)(\beta_{01}b_{02} - \beta_{02}b_{01})\end{matrix}\right] + V\delta\left(\beta_{01}\frac{\partial b_{02}}{\partial V} - \beta_{02}\frac{\partial b_{01}}{\partial V}\right)\right\}\right\}\left(\frac{\partial\Delta\beta}{\partial\lambda}\right)^{-1} \quad (9)$$

Where $k_0 = \frac{2\pi}{\lambda}$ is the free space wave vector, and $\eta = p_{12} - \sigma(p_{12} + p_{11})$, p_{11} and p_{12} are strain-optic coefficients for fused silica (0.12 and 0.27, respectively), σ is the Poisson ratio. $V = \frac{k_0 d_{core}}{2}\sqrt{n_{core}{}^2 - n_0{}^2}$ is the normalized frequency of the DMF, and d_{core} is the diameter of the fiber core, $\delta = \sigma(n_{core}{}^2 - n_0{}^2) + \frac{\eta}{2}(n_{core}{}^4 - n_0{}^4)$. β_{0i} and b_{0i} $(i = 1,2)$ are the propagation constant and normalized propagation constant of the LP_{01} mode and LP_{02} mode, respectively. The relation between them can be given as:

$$\beta_{0i}{}^2 = k_0{}^2[n_0{}^2 + b_{0i}(n_{core}{}^2 - n_0{}^2)] \quad (10)$$

In accordance with Eq. (8) and Eq. (9), the expressions of temperature sensitivity and humidity sensitivity differ for wavelengths on both sides of UWL. Moreover, if the wavelength to be tracked becomes nearer to UWL, the sensitivity becomes higher based on our previous studies [12]. Therefore, two peaks nearest UWL from both sides, denoted as peak1 and peak2, are selected to monitor the variations of the dual parameters. With the different responses to humidity and temperature of the two peaks, ΔRH and ΔT can be determined from the following matrix [16]:

$$\begin{bmatrix}\Delta T \\ \Delta RH\end{bmatrix} = \frac{1}{|k_{T1}k_{RH2} - k_{T2}k_{RH1}|}\begin{bmatrix}k_{RH2} & -k_{RH1} \\ -k_{T2} & k_{T1}\end{bmatrix}\begin{bmatrix}\Delta\lambda_{peak1} \\ \Delta\lambda_{peak2}\end{bmatrix} \quad (11)$$

Where k_{T1}, k_{RH1}, and k_{T2}, k_{RH2}, are the temperature sensitivity and humidity sensitivity of the peak1 and the peak2, respectively, and $\Delta\lambda_{peak1}$ and $\Delta\lambda_{peak2}$ are the wavelength shifts of the two peaks.

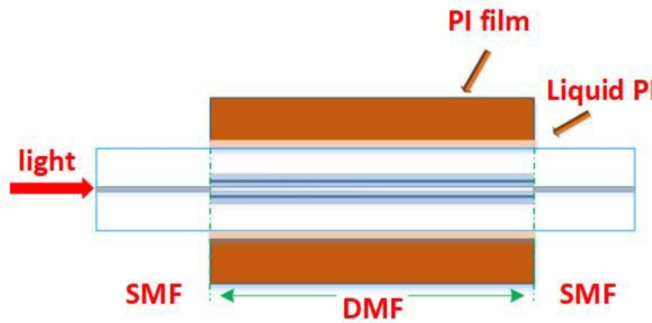

Fig.3. The structure of the proposed sensor.

For an interferometric sensor, it is well known that its sensitivity can be increased by introducing a reference interferometer with its free spectral range (FSR) close to the sensing one, which is called the Vernier effect. The response of the sensor to the measurand can be effectively enlarged in the combined spectrum, which has been applied extensively in humidity monitoring [18]-[20]. Generally, the sensitivity magnification factor M can be expressed as Eq. (12) if the refractive indexes of the sensing cavity and the reference cavity are assumed to be the same [21], [22]:

$$g = \frac{L_R}{L_S}, M = \frac{1}{|g-1|} \quad (12)$$

Where L_R and L_S are the cavity lengths of the reference interferometer and sensing one, respectively, and g is the scale factor of them. However, the conventional output spectrum of the Vernier effect scheme makes it hard to achieve a simultaneous measurement of dual parameters because of its periodicity. Therefore, the varied period Vernier effect is proposed to improve the sensitivity further and it will be generated in the next section when the reference SDS structure interferometer is involved.

III. Experimental Results And Discussion

A. The Fabrication Process Of The Sensing Interferometer

To fabricate the proposed sensing interferometer shown in Fig. 3, the following steps are carried out:
1. Stick one piece of PI film to the DMF of the SDS structure interferometer with the same type of liquid PI material;
2. Bond another piece of PI film with the first piece, which sandwiches the DMF in the middle of the PI films;
3. Put the combination of the DMF and PI films into the oven at 180 °C for an hour as the final curing.

The above steps are illustrated in Fig. 4.

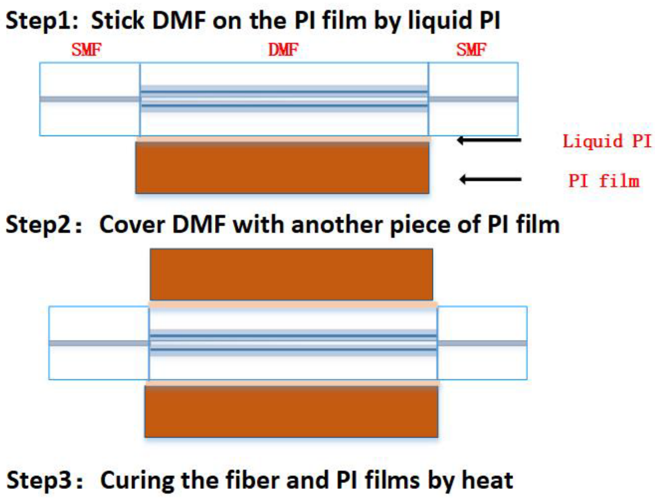

Fig. 4. The main steps of the fabrication process of the proposed sensor.

B. The Performance Of The Single Sensing Interferometer

To verify the validity of the single sensing dual modal interferometer for humidity measurement with temperature compensation, an experimental setup is established. The experimental diagram is illustrated in Fig. 5, where a supercontinuum light source (SLS) with a wavelength range from 1460 nm to 1620 nm is employed in the measurement. The light outputting from the light source will propagate to the sensor under the test, whose DMF length is 18.57 cm. The DMF length is determined based on the two adjacent peak wavelengths and the FSR of its corresponding spectrum. Then, the transmitted light will be led to an Optical Spectrum Analyzer (OSA, Yokogawa, AQ6370D) where the interferometric spectrum can be obtained. The sensor (the thickness of the PI film is selected as 0.1 mm as an example) is placed in a commercial constant temperature and humidity test chamber (Binder, KBF 720), which has a measuring range of 10% RH to 90% RH and -10 °C to 100 °C.

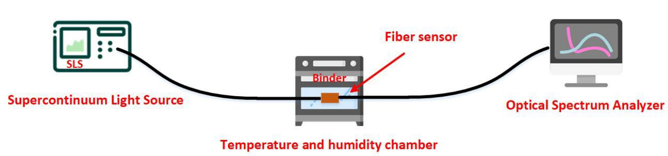

Fig.5. Schematic diagram of the experimental setup for simultaneous measurement of humidity and temperature with the sensing interferometer.

The response of the sensor to humidity and temperature is measured separately. First, the sensor is tested in a humidity-varying environment, while the surrounding temperature is maintained at 30 °C. The peaks closest to the UWL from both sides are selected as peak1 and peak2 (named PL and PR) to monitor the response of the sensor to the measurand, because they are expected to shift in the opposite directions as analyzed in the SENSING STRUCTURE AND MEASUREMENT PRINCIPLE part. Fig. 6 shows the variation of PL and PR for a humidity decrease from 60 %RH to 40 %RH with a step of 5 %RH. Both two peaks exhibit shifts in opposite directions as the RH increases, which is consistent with the theoretical analysis, with a sensitivity of 233.71 pm/%RH and 204.85 pm/%RH, respectively.

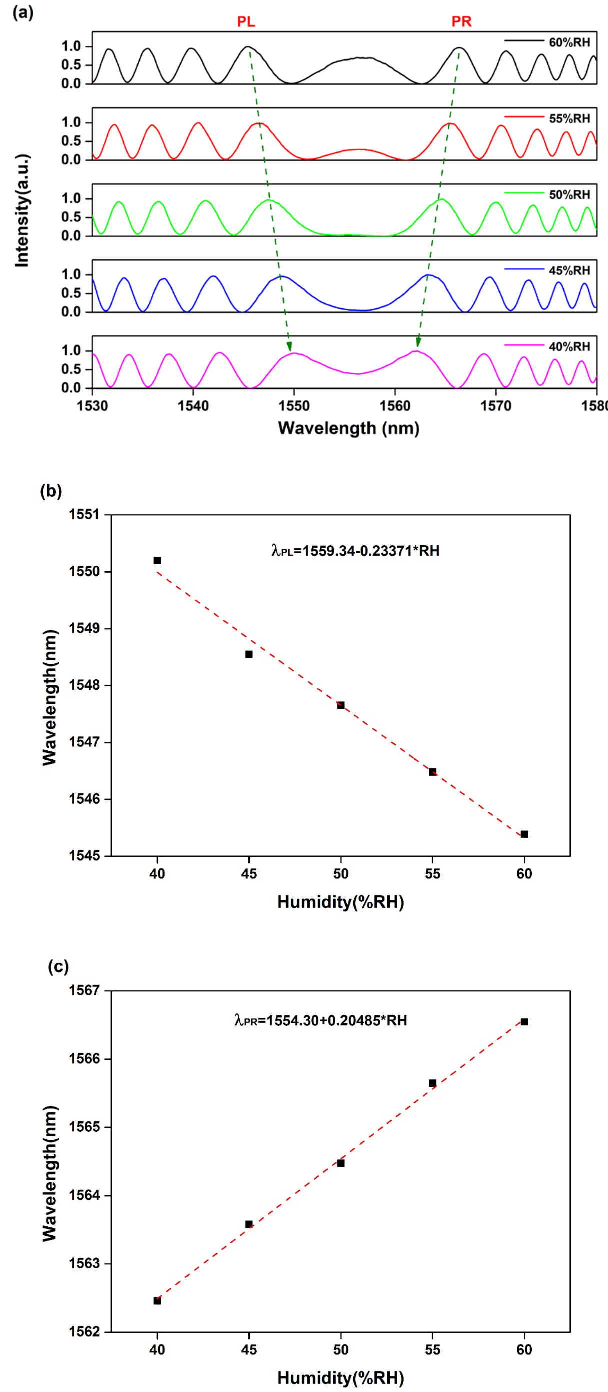

Fig.6. (a) The experimental normalized spectra of the single sensing interferometer when the humidity value ranges from 60 %RH to 40 %RH at a constant temperature of 30 °C. (b) Linear fit of the wavelength shift of PL. (c) Linear fit of the wavelength shift of PR.

Subsequently, the sensor is exposed to temperature values ranging from 50 °C to 30 °C at the constant humidity of 40 %RH. Fig. 7 depicts the evolution of PL and PR shifts as the surrounding temperature increases. PL presents a redshift, obtaining a temperature sensitivity of 364.68 pm/°C. While PR exhibits a blue shift with a temperature sensitivity of 315.94 pm/°C.

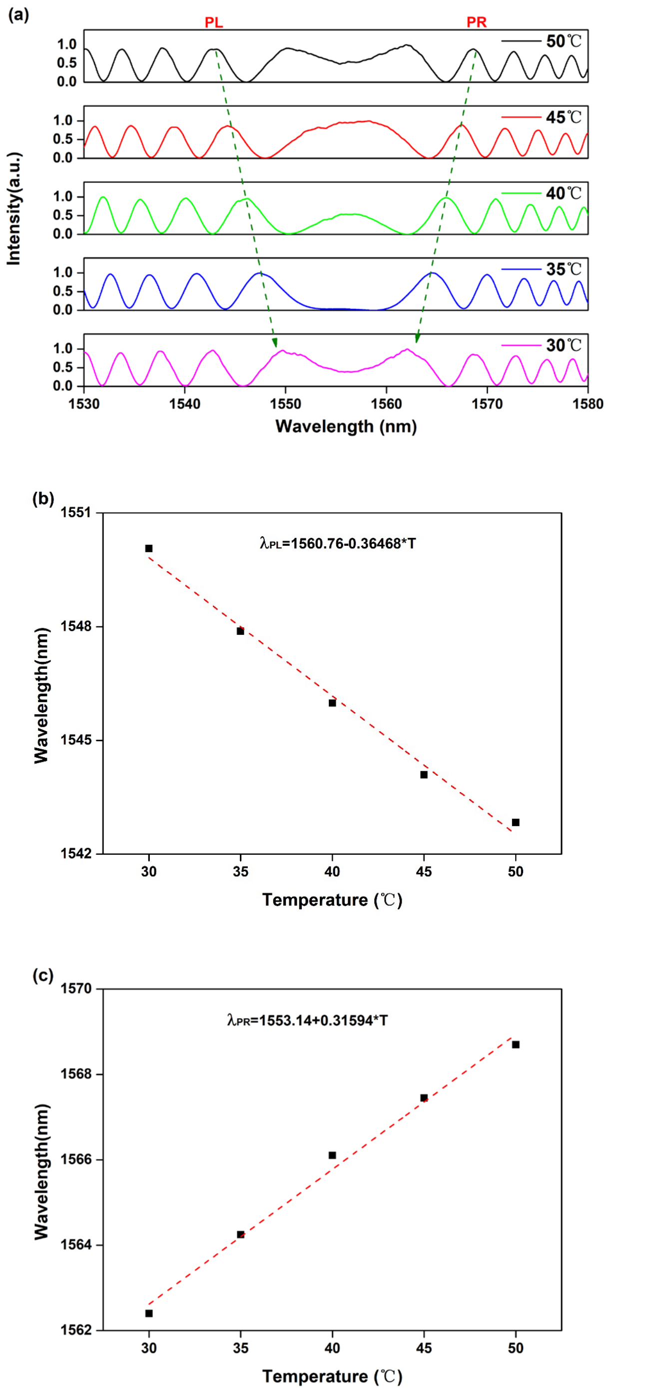

Fig. 7. (a) The experimental normalized spectra of the single sensing interferometer when the temperature value ranges from 50 °C to 30 °C at a constant humidity of 40 %RH. (b) Linear fit of the wavelength shift of PL. (c) Linear fit of the wavelength shift of PR.

Based on the above results, the coefficients of Eq. (11) can be determined as k_{RH1} = 233.71 pm/%RH, k_{RH2} = 204.85 pm/%RH, k_{T1} = 364.68 pm/°C, k_{T2} = 315.94 pm/°C. Therefore, the information of RH and temperature can be calculated by Eq. (13):

$$\begin{bmatrix} \Delta T \\ \Delta RH \end{bmatrix} = 0.0012 \begin{bmatrix} 204.85 & -233.71 \\ -315.94 & 364.68 \end{bmatrix} \begin{bmatrix} \Delta\lambda_{peak1} \\ \Delta\lambda_{peak2} \end{bmatrix} \quad (13)$$

When the proposed sensor is exposed to a wider humidity range (from 80%RH to 40%RH) or a temperature range (from 70°C to 30°C), the values of k_{RH1}, k_{RH2}, k_{T1} and k_{T2} can be determined as 225.98, 198.26, 360.02, and 311.89. This elucidates that the performance of the proposed sensor exhibits good consistency over a larger variation in measurands.

C. The Performance Of The Varied Period Vernier Effect-Based Sensor

To improve the sensitivity further, the Vernier effect is involved as a powerful tool. However, the conventional Vernier effect-based scheme can hardly achieve a simultaneous measurement of dual parameters due to the periodicity of its output spectrum, which limits its ranges for application. Therefore, a varied period Vernier effect scheme is demonstrated in this section, to measure humidity and temperature at the same time with the aid of the UWL in the output spectrum.

Similar to the traditional Vernier effect, a reference interferometer, whose FSR is close to the sensing one, is fabricated and paralleled with the sensing interferometer. The length of the DMF is 14.42 cm, which is fused with two SMFs on both sides. The sensing interferometer remains in the chamber, while the reference one is placed in another chamber with constant temperature and humidity. The corresponding experimental diagram is illustrated in Fig. 8.

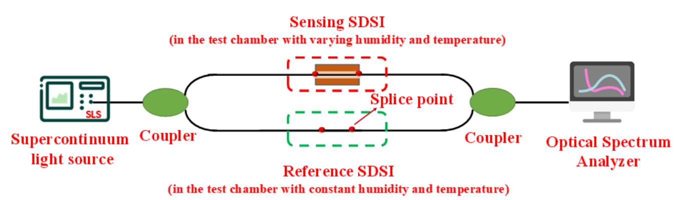

Fig. 8. The parallel configuration diagram of the proposed sensor based on the Vernier effect. (SDS interferometer is denoted as SDSI)

The humidity characteristic of the Vernier effect-based sensor is explored under the same humidity and temperature setting as the previous section B. The evolution of the output normalized spectra is illustrated in Fig. 9. By extracting the relative minimum values from the output spectrum and fitting them, the lower Vernier envelope can be obtained. The peaks of this lower Vernier envelope serve as valuable indicators for monitoring the measurand variation. Specifically, the peaks closest to the UWL from both sides are selected and identified as CPL and CPR to monitor the response of the sensor to the measurand.

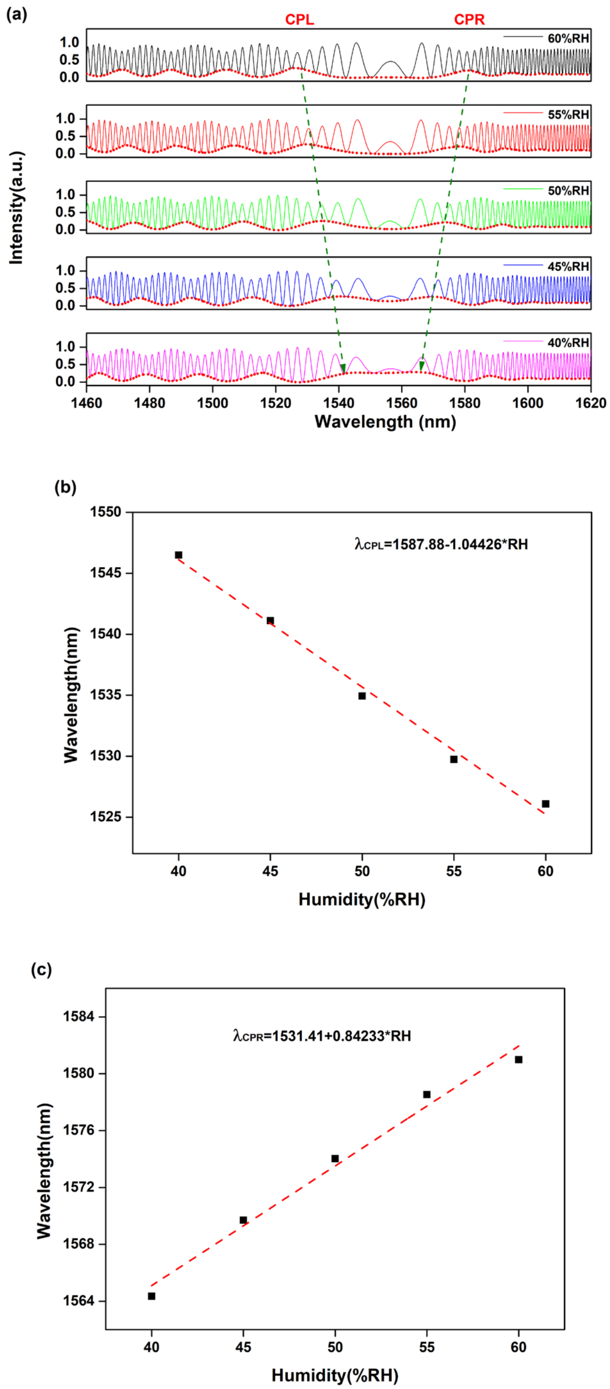

Fig. 9. (a) The experimental normalized spectra of the varied period Vernier effect-based sensor when the humidity value ranges from 60 %RH to 40 %RH at a constant temperature of 30 °C. (b) Linear fit of the wavelength shift of CPL. (c) Linear fit of the wavelength shift of CPR.

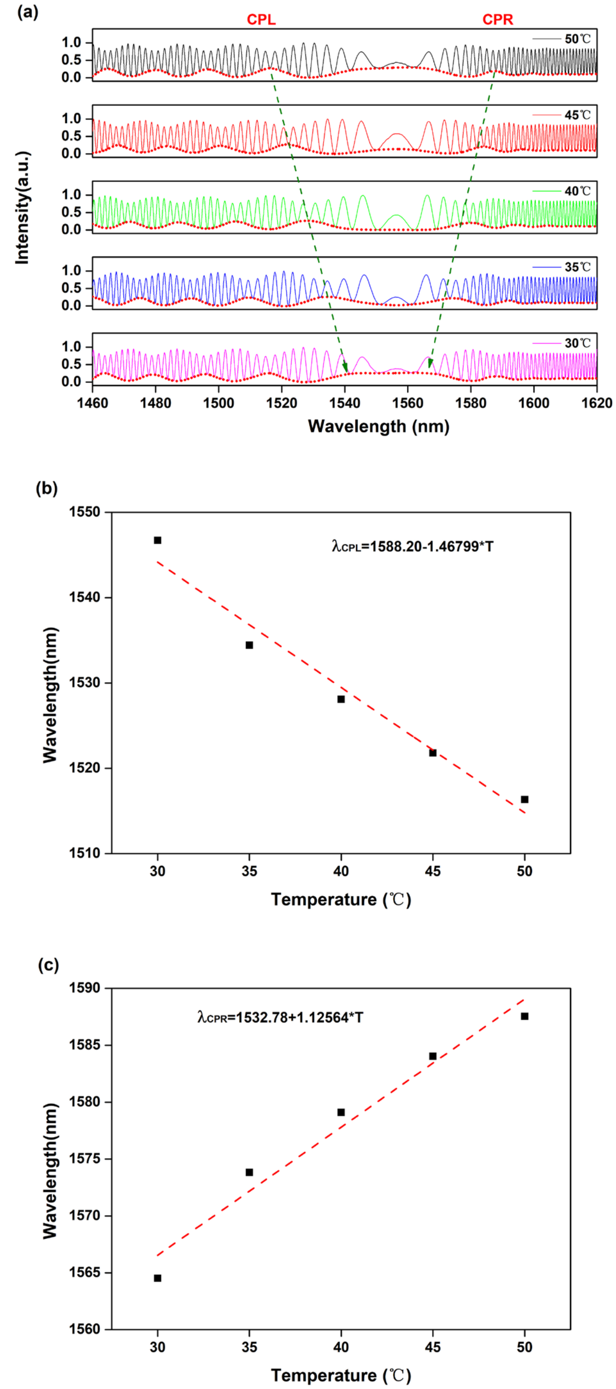

Fig. 10. (a) The experimental normalized output spectra of the varied period Vernier effect-based sensor when the temperature value ranges from 50 °C to 30 °C at a constant humidity of 40 %RH. (b) Linear fit of the wavelength shift of CPL. (c) Linear fit of the wavelength shift of CPR.

Subsequently, the temperature performance of the sensor is tested. CPL and CPR shift in the opposite direction, which is similar to that of the single interferometer and illustrated in Fig. 10.

According to the above results, the corresponding coefficients of Eq. (11) for the Vernier effect-based scheme can be determined as k_{RH1} = 1044.26 pm/%RH, k_{RH2} = 842.33 pm/%RH, k_{T1} = 1467.99 pm/°C, k_{T2} = 1125.64 pm/°C. Compared with the performance of the sensing one in the previous section B, the humidity and temperature sensitivities are both enhanced by 4 times, which is consistent with the theoretical result calculated by Eq. (12).

Furthermore, a comparison of the performance of the proposed sensor, and the same type of sensors reported in the existing literature, is shown in Table II.

TABLE II
THE COMPARISON OF DIFFERENT HUMIDITY AND TEMPERATURE OPTICAL FIBER SENSORS.

The structure of the sensor	Humidity sensitivity (pm/%RH)	Temperature sensitivity (pm/°C)	Reference
PI Coated FBG cascaded with a bare FBG	5	11	[23]
FBG partially bonded with PI thick films	14	19	[24]
Mach-Zehnder interferometer and Fabry–Perot interferometer	-132	370	[25]
Long period gratings array	530	460	[26]
The proposed sensing structure	1044	1468	-

By comparison, the proposed varied period Vernier effect-based sensor owns higher humidity sensitivity and temperature sensitivity than the traditional one with the aid of the thicker PI films. Besides, its UWL provides the ability to achieve highly sensitive measurements of dual parameters at the same time.

IV. Conclusions

In conclusion, a special DMF-based sensor bonded with thick PI films for highly sensitive humidity measurement and temperature compensation is proposed and demonstrated in this paper. Moreover, to our best knowledge, the varied period Vernier effect is applied in humidity measurement for the first time and the responses of the sensor to both measurands are enhanced greatly, which is consistent with the theoretical analysis. Furthermore, this work suggests the thick PI film-based humidity sensor owns a much higher sensitivity and a much lower manufacturing cost, compared with the conventional humidity sensors coated with thin PI coatings.

References

[1] B. Li, et al., "High sensitivity portable capacitive humidity sensor based on In2O3 nanocubes-decorated GO nanosheets and its wearable application in respiration detection," *Sens. Actuators B Chem.*, vol. 299, pp. 126973, 2019.

[2] X. Zhao, et al., "High Sensitivity Humidity Sensor and Its Application in Nondestructive Testing for Wet Paper," *Sens. Actuators B Chem.*, vol. 301, pp. 127048, 2019.

[3] A. Kapic, A. Tsirou, P. Verdini, and S. Carrara, "Humidity Sensors for High Energy Physics Applications: A Review," *IEEE Sens. J.*, vol. 20, no. 18, pp. 10335–10344, Sep. 2020.

[4] L. Alwis, T. Sun, and K.T.V. Grattan, "Optical fibre-based sensor technology for humidity and moisture measurement: Review of recent progress," *Measurement,* vol. 46, no. 10, pp. 4052-4074, 2013.

[5] D. Presti, C. Massaroni, and E. Schena, "Optical Fiber Gratings for Humidity Measurements: A Review," *IEEE Sens. J.*, vol. 18, no. 22, pp. 9065-9074, 2018.

[6] T. Yeo, et al., "Polymer-coated fiber Bragg grating for relative humidity sensing, " *IEEE Sens. J.*, vol. 5, no. 5, pp. 1082-1089, 2005.

[7] L. Alwis, et al., "Evaluation of the Durability and Performance of FBG-Based Sensors for Monitoring Moisture in an Aggressive Gaseous Waste Sewer Environment," *J. Lightw. Technol.*, vol. 35, no. 16, pp. 3380-3386, 2017.

[8] X. Rao, et al., "Review of Optical Humidity Sensors," *Sensors*, vol. 21, no. 23, 2021.

[9] Y. Han, "Relative Humidity Sensors Based on Microfiber Knot Resonators-A Review," *Sensors*, vol. 19, no. 23, 2019.

[10] Y. Wang, et al., "Simultaneous Measurement of Temperature and Relative Humidity Based on FBG and FP Interferometer," *IEEE Photon. Technol. Lett.,* vol. 30, no. 9, pp. 833-836, 2018.

[11] S. Wu, et al., "An open-cavity Fabry-Perot interferometer with PVA coating for simultaneous measurement of relative humidity and temperature," *Sens. Actuators B Chem.*, vol. 225, pp. 50-56, 2016.

[12] C. Lu, et al., "Label Free All-Fiber Static Pressure Sensor Based on Vernier Effect With Temperature Compensation, " *IEEE Sens. J.*, vol. 20, no. 9, pp. 4726-4731, 2020.

[13] C. Lu, X. Dong, and J. Su, "Detection of Refractive Index Change From the Critical Wavelength of an Etched Few Mode Fiber," *J. Lightw. Technol.*, vol. 35, no. 13, pp. 2593-2597, 2017.

[14] Q. Li, C. Lin, P. Tseng and H. Lee, "Demonstration of high extinction ratio modal interference in a two-mode fiber and its applications for all-fiber comb filter and high-temperature sensor," *Opt. Commun.*, vol. 250, no. 4-6, pp. 280-285, 2005.

[15] N. David, P. Wild, and N. Djilali, "Parametric study of a polymer-coated fibre-optic humidity sensor," *Meas. Sci. Technol*, vol. 23, no. 3, 2012.

[16] C. Lu, et al., "Studies on Temperature and Strain Sensitivities of a Few-Mode Critical Wavelength Fiber Optic Sensor," *IEEE Sens. J.*, vol. 19, no. 5, pp. 1794-1801, 2019.

[17] J. Zhang, et al., "An optical fiber sensor based on polyimide coated fiber Bragg grating for measurement of relative humidity," *Opt. Fiber Technol.,* vol. 61, 2021.

[18] C. Zhou, et al., "High-sensitivity relative humidity fiber-optic sensor based on an internal–external Fabry–Perot cavity Vernier effect," *Opt. Exp.*, vol. 29, no.8, pp. 11854-11868, 2021.

[19] L. Hou, et al., "Ultra-Sensitive Optical Fiber Humidity Sensor via Au-Film-Assisted Polyvinyl Alcohol Micro-Cavity and Vernier Effect," *IEEE Trans. Instrum. Meas.*, vol. 71, pp. 1-9, 2022.

[20] Y. Wang, et al., "Signal processing integrated with fiber-optic Vernier effect for the simultaneous measurement of relative humidity and temperature," *Opt. Exp.,* vol. 31, pp. 28636-28648, 2023.

[21] Y. Guan, and X. Dong, "Reconfigurable highly-sensitive interferometric sensor with Vernier effect and a virtually tunable reference cell," *Opt. Commun.,* vol. 535, 2023.

[22] Y. Guan, J. Yang, B. Yin, and X. Dong, "Study of the Sensitivity Limit of Vernier Effect and a Novel Tracking Method of Vernier Envelope," *IEEE Photon. Technol. Lett.,* vol. 35, no. 2, pp. 77-80, 2023.

[23] B. Rente, et al., "A Fiber Bragg Grating (FBG)-Based Sensor System for Anaerobic Biodigester Humidity Monitoring," *IEEE Sens. J.*, vol. 21, no. 2, pp. 1540-1547, 2021.

[24] Y. Guan, et al., "Sensor for Simultaneous Measurement of Temperature and Humidity Based on a Chirped Fiber Bragg Grating Partially Bonded With Thick Polyimide Film," *IEEE Sens. J.*, vol. 23, no. 20, pp. 24583-24590, 2023.

[25] R. Tong, Y. Zhao, H. Zheng, and F. Xia, "Simultaneous measurement of temperature and relative humidity by compact Mach-Zehnder interferometer and Fabry-Perot interferometer," *Measurement,* vol. 155, Apr. 2020.

[26] J. Hromadka, et al., "Simultaneous in situ temperature and relative humidity monitoring in mechanical ventilators using an array of functionalised optical fibre long period grating sensors," *Sens. Actuators B Chem.*, vol. 286, pp. 306-314, May 2019.